IOSR Journal of Pharmacy and Biological Sciences (IOSR-JPBS)
e-ISSN:2278-3008, p-ISSN:2319-7676. Volume 13, Issue 5 Ver. III (Sep – Oct 2018), PP 01-10
www.iosrjournals.org

TiO_2 And Pt/Pd Doped TiO_2 Upconversion Nanoparticles For Photodynamic Biomedical Applications

Veena.V [1]*, K.H. Shivaprasad [1], K.S. Lokesh [1], A.M.Krupanidhi [2]
1 Department of Chemistry, Vijayanagara Sri Krishnadevaraya University, Ballari.
2 Bapuji Pharmacy College, Davangere, Karnataka.
Corresponding Author: Veena.V

Abstract: *Nanoparticles have received much attention in present scenario due to their application in cancer therapy. Based on clinical efficacy, TiO_2 has a very wealthy data related to cytotoxicity. The present study involves novel synthesis of nanocrystalline powders of virgin and also the ones doped with Pt, Pd and bimetallic Pt/Pd. The synthesized nanocrystalline TiO_2 were characterized by UV, IR, XRD, SEM, and DLS. The Characterization results demonstrated that doping decreases the band gap or introduces intra-band gap states leading to photosensitizer (PS) systems that exhibit enhanced efficiency under visible light. The prospects of using newly syntheised nanocrystalline powders of TiO_2 in biomedical studies revealed that the nanoparticles have significant antibacterial, antifungal and antitumor activity under visible light. The observed anticancer activity of analogues was dose dependent and there was a significant increase in percentage of life span in treated mice with doped TiO_2 nanoparticles i.e. 52.38% to 57.14% against EAC-cells. Hence, the synthesized nanoparticles possess significant biomedicinal applications.*

Key words: *Nanoparticle TiO_2, doped with Pt,Pd , both Pt/Pd ,EAC, SGD, ILS.*

Date of Submission: 14-09-2018 Date of acceptance: 29-09-2018

I. Introduction

Cancer is among the leading causes of death in the world wide, with million incidences and million deaths estimated every year [1]. In order to cure the various types of malignancy, several therapeutic routes have been adopted in the recent past. Among them chemotherapy, radiotherapy (XRT), photodynamic therapy (PDT), target drug delivery systems (DDSs), surgical intercessions and other conventional methods are very common [2,3]. Indeed, metals are used extensively in cancer diagnosis, therapy and the lanthanides occupy an important niche in these areas [4].The development of new drug delivery system which makes use of a therapeutic agent or metal nanoparticles that bind/hold therapeutic agent and can be delivered to an internal target site in a controlled manner, is one of the most active research areas in the field of medical applications as nanomedicines. Particularly, stimuli-triggered drug delivery systems (DDSs) that can release the bioactive compounds with precise control over timing, site, and dosage of the released therapeutic agent upon illumination of certain radiations have received attention in past few years. [5–7]. As from literature reviews, both UV and visible light radiations have poor tissue penetration depth, and prolonged exposure to UV can cause severe cellular photodamage that hamper their practical applications in DDSs [8–10]. To facilitate lower phototoxicity and increase the depth of tissue penetration, near infrared radiations (NIR-to-UV/visible) up-conversion nanoparticles (UCNPs) have emerged as potential remote-controlled method, which activate the photoreaction of photosensitive molecules [11, 12].

TiO_2 nanoparticles (NPs) have wide-spread application as additives in sunscreen products, paints, printing ink, rubber, paper, sugar, cement, toothpaste, film plastic packaging, self-cleaning sanitary ceramics [13], bio-medical ceramic, implanted biomaterials ,antimicrobial in biomedical fields including drug delivery, cell imaging, photodynamic therapy and biosensor [14,15] which have assumed increasing importance, and concerns, due to their chemical stability, photocatalytic efficiency, biocompatibility, strong oxidizing/reducing ability and low cost [16].Owing to their widespread use, some studies suggest that TiO_2 NPs induce inflammation, cytotoxicity and genotoxicity [17–19] and also some have been reported that TiO_2 NPs were not toxic or least toxic to several cell lines [20–22].Thus conflicting reports are available on toxicological effects of TiO_2 NPs which could be due to the importance of their size and surface area available which effects

physicochemical properties and functionalities that are different from their bulk counterparts [22, 23]. While, till today there is a need for understanding biocompatible potential of these nanoparticles.

The majority of pristine TiO_2 nanoparticles are active under UV light excitation, hole-electron pairs are generated, which result in the formation of reactive oxygen species (ROS) via the redox reactions of oxygen or water molecules at the TiO_2 surface, due to their large band gap energy (3.2 eV for anatase) the photocatalytic efficiency of TiO_2 NPs are reduce considerably [24, 25].Additionally, UV-mediated production of reactive oxygen species has a short life span and hence, they cannot offer nonstop or prolonged cancer killing effect [26,27]. Furthermore, when doped or modified with different methods, TiO_2 nanoparticles may become an attractive photosensitizer (PS) systems that exhibit enhanced efficiency due to increase in their surface defects and extend their spectral response under visible light irradiation [28].

Doping of TiO_2 has been an important approach in band gap engineering to change the optical response of the photosensitizer (PS). For example, doping of TiO_2 NPs with noble metals such as Ag, Au or Pt can efficiently decrease the electron-hole recombination pair's as the band gap is decreased which enhance the photocatalytic activity and simultaneously extend their light response towards the visible region because of their d electron configuration [29]. Generating ROS and their potential applications by doped TiO_2 NPs which make them active under visible light have been recently investigated in killing of microbial communities [30, 31]. Thus, some studies have shown that doped TiO_2 can kill bacteria without any light illumination and can be activated under normal light. [32, 33].

Nevertheless, despite of the rapid developments in photosensitizer (PS) systems for cancer diagnosis and therapy,the potential long term toxicity and stability of photo responsive materials and heavy metal dopants needs more advanced evaluation for in vivo applications. The heavy metals are expected to reduce the electron-hole pair recombination and enhance the photocatalytic efficiency of TiO_2. Thus, the aim of this present study is to synthesize undoped TiO_2 and metallic and bimetallic doped (M=Pd, Pt, Pt/Pd) TiO_2 nanoparticles by Solution combustion method and to study their potential uses like antibacterial, antifungal and anti-neoplastic(anticancer)activities under visible light. Thus, the unique character of these nanoparticles due to their small size, shape, and charge, as well as the cell type being treated and quantum size effect could make TiO_2 nanoparticles biocompatible.

II. Materials and Methods

2.1. Chemicals and Materials

Titanium tetra isopropoxide (98%), Platinum chloride (99.9%) and Palladium chloride (99.9%) were purchased from Sigma Aldrich. Glacial acetic acid (100%), Mueller –Hinton agar, Potato Dextrose agar were purchased from Merck. Other reagents were of analytical grade and purchased from SD fine Chemical's and used as received without further purification.

2.2. Synthesis of doped TiO_2 nanoparticles

Titanium dioxide (TiO_2) and doped TiO_2 nanoparticles have been prepared by solution combustion method. An aqueous combustion mixture of 2.87g of $TiO(NO_3)_2$ which was prepared from $Ti(OC_3H_5)_4$, in which the number of equivalent $TiO(NO_3)_2$ is equal to titanium tetra isopropoxide and 0.8g of glycine as fuel in 15ml water was introduced into a 300 ml Pyrex dish and preheated to 350^{o}C for 1h in a muffle furnace. The TiO_2 nanoparticles were doped by dopants i.e. 0.3mmol of $PdCl_3$ for Pd doping, 0.3 mmol $(NH_3)_4Pt\ (NO_3)_2$ for Pt doping and 0.3 mmol mixture of both $PdCl_3$ and $(NH_3)_4\ Pt\ (NO_3)_2$ were used for bimetallic doped nanoparticles synthesis. The solution mixture was calcinated in a preheated muffle furnace at 350 ^{o}C for 1 h.

2.3. Antibacterial activity and antifungal activity

Agar well diffusion assay method was used to study antibacterial activity and antifungal activity of nanoparticles. Antibacterial activity was performed against four microorganisms, Klebsiellapneumonia, Pseudomonas aeruginosa and Escherichia coli. Antifungal activity was performed against two fungi, Candida albicans and Aspergillus Niger. Muller Hinton agar media for antibacterial activity and Potato dextrose agar media for antifungal activity were prepared, sterilized and aseptically transferred to Petri plates. These Petri plates were kept for solidification of media and later kept in incubator overnight to confirm that the Petri plates are free from contamination. These Petri plates were then inoculated with test organisms and wells were prepared for loading test samples. The concentrations of 50 mg/ml and Tetracycline 25 µg/ml, Griseofulvin 25 µg/ml test and standard were loaded in different wells to evaluate their antibacterial susceptibility. Zones of inhibition were measured using Hi media scale after 24 h of incubation at 37^{0}C. All the experiments were performed in triplicate and results were recorded as mean ±standard deviation.

2.3. a. Minimum inhibitory concentration (MIC)

The micro dilution method for estimation of MIC values was carried out to evaluate the antimicrobial activity. The MIC values were determined on 96-well micro dilution plates according to published protocols [34].

2.4. In-vivo anticancer activity of TiO_2 and doped nanoparticles

Acute toxicology test

Acute toxicity study was performed using albino mice and doses were fixed as per OECD guideline No.423 and adopted CPCSEA protocol. Albino mice of either sex (8-10 weeks old) weighing 20-25 g mice were obtained from S.S Institute of Medical Sciences and Research Center, Davanagere.

Animals were maintained in the pathogen-free authorized facility where temperature was maintained at 20–22°C, relative humidity at 50–60%, and with 12 h dark/light cycles. All animals were provided water and mouse (rodent) chow. For tumour inoculation on day 0 (DO), the 0.5 ml of a 1:10 Ehrlich Ascites Tumour crushed in Hank's balanced salt solution (HBBS) were inoculated by the intra peritoneal route in albino mice as shown in (figure 1). The treatment began the day after tumour inoculation, and test compounds and vehicle were administered, using (n=6) mice per test group. Routinely, the drug was administered six times in a day after tumour inoculation. In each group, trail mice were checked daily for any adverse clinical reactions which were noted and deaths recorded. Mice were weighed 2-4 times daily during treatment and once weekly thereafter. TiO_2 and doped TiO_2 (M=Pd, Pt, Pt/Pd) nanoparticles were suspended in normal saline solution to yield a stock and then diluted in 0.9% NaCl solution. Prior to use for injection, the suspension was stirred to assure no significant agglomeration. Immediately after this step for the evaluation of anticancer activity, albino mice were subdivided into (n=8) groups. Tumours are measured by Screw gauge twice and tumour area (mm^3) were estimated. Results are presented for experiments involving (n=6) mice per experimental group as shown in Table 1.

Figure 1: Inoculation of EAC tumour

Table 1. Anticancer activity of the undoped and doped TiO_2 nanoparticles

SL.No	Nanoparticles	Quantity of nanoparticles injected
1	Control	Ehrlichsascites Carcinoma (EAC) induced by the i.p. route in albino mice received solvent p.o(per oral root)
2	T1(TiO_2)	(EAC) 10µg/kg
3	T2(Pd/TiO_2)	(EAC) 10 µg /kg
4	T3(Pt/TiO_2)	(EAC) 10 µg / kg
5	T4 (Pd/Pt/TiO_2)	(EAC) 10 µg/kg
6	T1 (TiO_2)	(EAC) 20 µg/kg
7	T3 (Pt/TiO_2)	(EAC) 20 µg/kg
8	T4 (Pd/Pt/TiO_2)	(EAC) 20 µg/kg

2.4. a. Evaluation of antitumor activity

Life Span Mortality was noted every day and mice surviving for at least 45 days were considered as cured and were included in the calculation of the median life span. Drug efficiency is expressed by T/C, the median life span(MLS),Specific tumour growth delay (SGD), Tumour regressions was defined as; partial regressions (PR) if the tumour volume decreased to 50% or less than that, at the beginning of the treatment, without dropping below measurable size. Drugs were administered with in different schedules and increased life span

ILS are then determined. Where (MTD) is Maximum tolerance dose and (TI) Therapeutic index, (SGD>1) corresponds to minimal level of activity were calculated as follows using formula as given below,

$$MLS = \frac{Dm + (Mm\text{-number of mice dead before Dm})}{\text{Number of mice dead on Dm}}$$

$$T/C\% = (\text{MLS of treated animals}/ \text{MLS of animals}) \times 100$$

Or

By the increase in life span $ILS\% = 100 \times (T-C)/C$

$$\text{SGD for Ehrlich Ascites Tumour model} = \frac{Td\ (\text{drug-treated group})}{Td\ (\text{vehicle-treated group})}$$

Use of (Mm) separates into two identical groups (one group, including the mice that died before Mm, the other group including those who died after) and the median day (Dm) is the day Mm died. Treatment efficiency is assessed in terms of the nanoparticles effects on the tumour volumes where (T) tumour bearing mice relative to the (C) control vehicle-treated mice. For evaluation, criteria were used in parallel's being the tumour doubling time of drug (treated and control) groups, defined as the time in days required for the tumours volume to double.

2.5 Characterization

The morphological features of the synthesized nanoparticles were studied by using SEM and elemental analysis was carried out using energy dispersive X-ray spectroscopy attached to SEM (Carl Zeiss Microscopy, EVO 10, Germany) . The double coated conductive carbon tape was used as adhesive and pasted on stub. Thin layer of dried nanoparticle (~0.2 mg) was placed on adhesive surface. Sample holder was kept in vacuum chamber and then placed in sample chamber for SEM analysis. Visible spectrophotometer (Perkin Elmer, Lambda 35, Germany) was used to record the absorption spectra of the samples in the wavelength range between 200-800 nm and the amount of the radiation absorbed was recorded. FTIR spectra of undoped and doped TiO_2 were recorded using Shimadzu FTIR spectrophotometer. Samples were analyzed by KBr pellet technique in the range 450–4000 cm^{-1} at resolution of 4 cm^{-1}.X-ray diffraction (PXRD) data for the phase analysis of undoped and doped TiO_2 have been recorded on Rigaku theta type X-ray diffractometer using Cu-Kα radiations which was operated at 40 KV voltage, 30 mA current, and 20 to 70 (2θ) range. The average crystallite sizes of samples were quantitatively calculated using Scherer formula after correcting the instrumental broadening. Dynamic light scattering (DLS) also known as photon-correlation spectroscopy or quasielastic light scattering was used to determine the size-distribution profile of small particles in suspension or solution [35], as well as other physicochemical properties such as zeta potential. Malvern Zetasizer was used to study the zeta potential and particle size distribution of undoped and doped nanoparticle dispersion solution. The nanoparticles were appropriately diluted using deionized water and analyzed.

III. Result

Titanium dioxide (TiO_2) and doped TiO_2 nanoparticles have been prepared by solution combustion method. In the typical synthesis of TiO_2 nanoparticles, the stoichiometry of the combustion mixture was calculated based on the total oxidizing to reducing valences of the oxidizer and fuel, keeping oxidizer/ fuel ratio unity, using the concepts of propellant chemistry. The synthesized doped nanoparticles have the stoichiometry as $Ti_{0.97}Pd_{0.03}O_{2-\delta}$, $Ti_{0.97}Pt_{0.03}O_{2-\delta}$ and $Ti_{0.9797}Pd_{0.005}Pt_{0.025}O_{2-\delta}$.

3.1 Scanning electron microscopy studies:

SEM images of the undoped and doped TiO_2 are as shown in the (figure 2). As observed, the surface morphology of the undoped and doped TiO_2 nanoparticles have remarkably changed that are voluminous, weakly agglomerated and more porous after doping. The voids and pores present in the sample are due to the large amount of gases produced during the combustion synthesis [36].

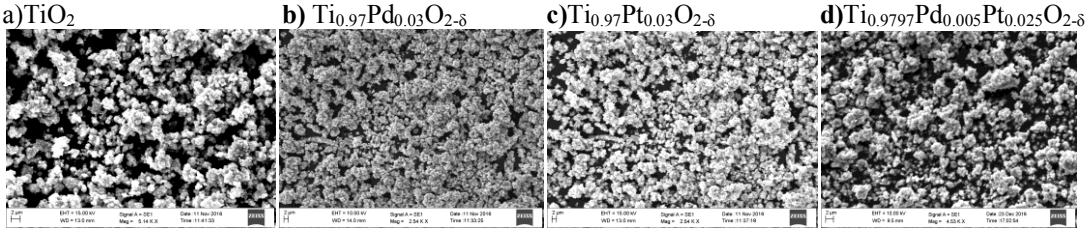

Figure 2: SEM images of TiO_2 and M/ TiO_2 (M=Pd, Pt, Pt/Pd) doped nanoparticles

3.2 Fourier Transform Infrared Spectroscopy (FTIR)

The FTIR spectra of undoped TiO_2 and M/ TiO_2 (M=Pd, Pt, Pt/Pd) doped nanoparticles are shown in (figure 3). The peaks at 468 cm^{-1} and 650 cm^{-1} are for Ti- O and -OTi-O bonding. The broad peaks appearing at 3400-3700 cm^{-1} are assigned to vibrations of –OH groups and band centered at 1618 cm^{-1} is characteristic of O-H stretching band. The peaks at around 1163-1185 cm^{-1} could be ascribed to nitrogen oxide species. However, the vibration bands between 1300 cm^{-1} and 1400 cm^{-1} are mainly assigned to the chemisorbed or physiosorbed H_2O and CO_2 molecules on the surface of the compound. Upon addition of dopants, a small shift was detected for the stretching vibration of Ti–O [39].

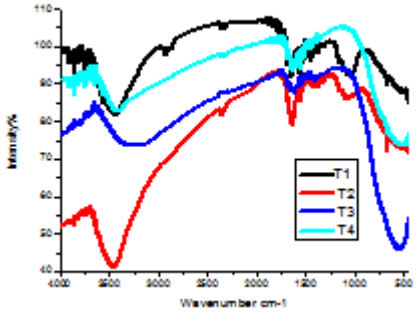

Figure 3 : FTIR spectra of TiO_2 and M/ TiO_2 (M=Pd, Pt, Pt/Pd) doped nanoparticles

3.3 UV-Vis absorption spectra of TiO_2 nanoparticles and their doping effect with noble metals

The UV-Vis spectrum (figure 4) indicates a strong light absorption in the UV region. The increase in the absorption peak intensity in the visible region with the addition of Pd, Pt and bimetallic Pt/Pd was observed. Additionally, it is observed that a significant red shift was induced by Pd, Pt and both Pt/Pd doping in TiO_2 nanoparticles which might be due to the formation of an intra-gap energy level inside the band gap of TiO_2 nanoparticles. The band gap energy (Eg) of the material was calculated using the formula Eg(ev) =1240/λ [37]. From figure 4 it is clear that the Pd, Pt and Pt/Pd doping into TiO_2 results in an increase in the visible light response and that the doping effectively extends the absorption from UV to visible region by the reduction of the band gap value [36, 38].

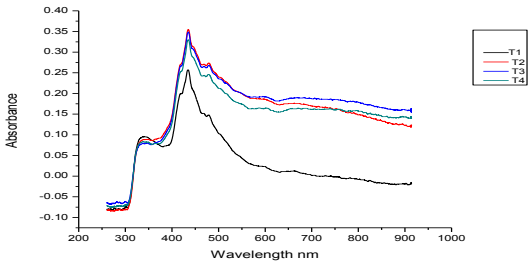

Figure 4 : UV spectra of TiO_2 and M/ TiO_2 (M=Pd, Pt, Pt/Pd) doped nanoparticles

3.4 PXRD analysis

The X-ray diffraction (XRD) patterns of undoped and doped TiO_2 nanoparticles synthesized by solution combustion method are shown in (figure 5) respectively. All the peaks in the XRD pattern can be indexed to an anatase phase of TiO_2 and the diffraction pattern were in good agreement with JCPDS No: 21-1272. For TiO_2 (anatase type), the major peaks observed at 2θ values of 25.3,38.3,48.20,55.0, 62.6,69.5 and 75.1 degrees which are assigned to (101),(004) (200),(105) (204), (116) and (215) reflections of anatase respectively. The intensity of diffraction peaks corresponding to (101) crystal plane of each sample was selected for calculating the crystal size by using the Scherer equation P= kλ/βcosθ. Particle size (P) was estimated based on the peak width (B) giving a shape factor (k) of 0.9, λ (the wavelength of the Cu-Kα1 X-ray radiation of 0.1541 nm), β (full peak width at half maximum corrected for instrumental broadening) [42]. For the peak (101) reflection at 2θ (25.40)

by using the full width at half maximum (fwhm), the particle size of doped and undoped nanoparticles are illustrated in the table 2.

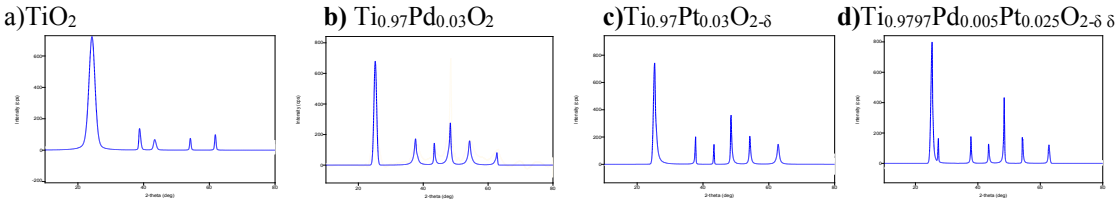

Figure 5: XRD patterns of TiO_2 and M/ TiO_2 (M=Pd, Pt, Pt/Pd) doped nanoparticles

Table 2. Rietveld refined lattice parameters and crystalline size of undoped and doped TiO_2

Sl.No	Sample	Crystalline size(nm)	A	C	Cell volume	R_f	R_B
1)	TiO_2	13±8nm	3.779(1)	9.497(1)	135.6	2.8	2.
2)	Pd/TiO_2	13±2nm	3.778(1)	9.473(0)	135.5	2.7	2.5
3)	Pt/TiO_2	14±2nm	3.779(0)	9.485(1)	135.4	2.5	2.3
4)	Pt/Pd/ TiO_2	13±2nm	3.780(0)	9.507(0)	135.45	2.6	2.9

3.5 Zeta potential and particle size distribution:

In this study, DLS was used to characterize the size and zeta potential. The distribution of the size as a function of intensity is shown in (figure 6). The average size of TiO_2 and M/ TiO_2 (M=Pd, Pt, Pt/Pd) colloidal dispersion solution was found to be about 13±8nm. The Zeta potential of the four dispersions was of the same order of magnitude, which coincided with the results of XRD particle size measurement. The zeta potential of the dispersions was also quite similar i.e. -23.1mV to -22.9mV for all the dispersion solution, indicating that doped metal ions were substituted directly in Ti^{+4} sites.

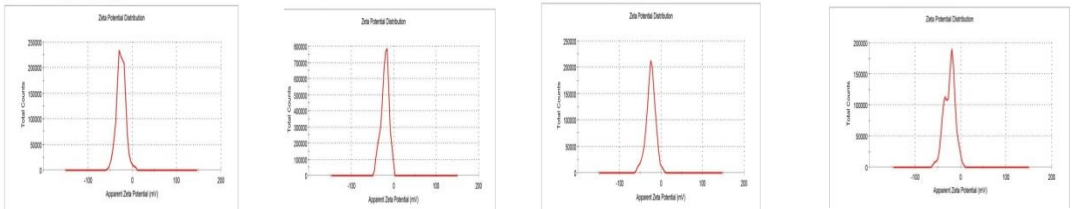

a)TiO_2**b)**$Ti_{0.97}Pd_{0.03}O_{2-\delta}$**c)**$Ti_{0.97}Pt_{0.03}O_{2-\delta}$ **d)**$Ti_{0.9797}Pd_{0.005}Pt_{0.025}O_{2-\delta}$

Figure 6: Zeta potential images of TiO_2 and M/ TiO_2 (M=Pd, Pt, Pt/Pd) doped nanoparticles

3.6 Well Diffusion and Minimum Inhibitory Concentration

Antimicrobial activity of TiO_2 and M/ TiO_2 (M=Pd, Pt, Pt/Pd) doped nanoparticles were investigated by well diffusion method against three bacterial and two fungal strains. The results of zone inhibition method has been described in (figure 7) indicates that NPs shows good inhibition zone. The micro dilution method for estimation of MIC values was carried out to evaluate the antimicrobial activity. The MIC values were determined on 96-well micro dilution plates according to published protocols [51]. The MIC observed in the present study for synthesized TiO_2 and M/ TiO_2 (M=Pd, Pt, Pt/Pd) doped nanoparticles are presented in the table 3.

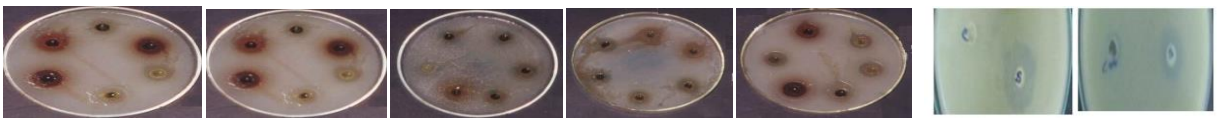

Fig:A Fig: B

Figure 7: Images of TiO_2 and M/ TiO_2 (M=Pd, Pt, Pt/Pd) doped nanoparticles showing inhibition zones of nanoparticles on E.coli, Pseudomonas aeruginosa, Kleibsiella pneumonae, Candida albicans, Aspergilus Niger and (Fig:A-Tetracyclin Fig: B-Griseofulin.)

Table 3: **Antibacterial and antifungal activity of TiO_2 and M/ TiO_2 (M=Pd, Pt, Pt/Pd) doped nanoparticles**

Organisms	**Zone of inhibition in mm Different fraction extracts of 50mg/ml**					
	Standard – **Tetracycline**	**Griseofulvin**	TiO_2	TiO_2 /Pd	TiO_2 /Pt	TiO_2 /Pd/Pt
E-coli	32 ±0.30	-	18.6± 0.35	24.0±0.78	29± 0.31	31.0±0.20
P-aeruginosa	34±0.62	-	24.0 ±0.8	24± 0.31	29± 0.31	34± 0.31
K-pneumonae	30±0.84	-	28.0 ±0.6	26± 0.52	30± 0.6	35.0±0.20
C-albicans	-	34± 0.26	22.0 ±0.6	25± 0.3	30± 0.26	34± 0.6
A-niger	-	40± 0.68	24.0 ±0.6	26± 0.3	38± 0.42	42.± 0.26

3.7 In vivo acute toxicology test study of TiO_2 and doped nanoparticles

An induction of apoptosis in cancer cells is considered as a new focus in the discovery of anti-cancer drugs. The treatment groups were assessed by determination of percentage of increase lifespan (ILS %) and standard growth delay (SGD) of tumour volume was measured in all the groups, table 4 which summarises that the virgin and doped TiO_2 nanoparticles which were synthetic analogues of TiO_2. Similarly the percentage of increase in the life span (ILS %) were 33.33%, 38.09%, 52.38% and 57.14% for TiO_2 and M/ TiO_2 (M=Pd, Pt, Pt/Pd) doped nanoparticles.

Table 4: Anticancer activity of TiO_2 and M/ TiO_2 (M=Pd, Pt, Pt/Pd) doped nanoparticles p.o against the EAC

Treatment Schedule	MTD (mg/kg-1)	TI	Dose (mg/kg-1)	SGD	ILS %	Wt.(gms) changes in treatment groups		Survival
						0 Day	After 11 day	
D1	>100	10	10	0.66	14.28	32.00	29.16	3/6
D1	>200	10	20	0.08	19.04	30.83	28.33	4/6
D 1, 3, 5, 7, 9, 11	>100	10	10 10 10	0.29 0.20 -0.20	33.33 38.09 52.38	31.00 32.05 32.00	29.50 30.00 29.00	5/6 6/6 6/6
D 1, 3, 5, 7, 9, 11	>200	10	20 20	0.20 -0.41	38.09 57.14	28.00 31.16	27.00 29.00	5/6 6/6

IV. Discussion

The worldwide prevalence of cancer leads to an increase in attempts which are aiming for the development of innovative and effective photocatalyst for treatments of cancer cells. In combustion synthesis, it's well known that the morphological characteristics of the prepared powder are strongly dependent on the heat and gases generated during the complex decomposition. Large volume of gases facilitates the formation of tiny particles while the heat released is an important factor for crystal growth. The combustion takes place after the dehydration and the solid product left behind are very fine nanoparticles. Thus the agglomerations of the nanoparticles in the (figure 2) of SEM images which are usually explained, as a common way to minimize their surface free energy. However, some investigators suggest that agglomerations are assigned to the presence of organic radicals that act as binders. Further the presences of functional groups were confirmed from FTIR Spectra. FTIR spectra were recorded in the range of 500–4000 cm^{-1} for undoped and doped TiO_2 nanoparticles. When metal ions are doped to the surface of TiO_2, the absorption band transforms and simultaneously new absorption band appears. The broad bands in around 400 and 800 cm^{-1} (figure 3) are assigned to the Ti-O and O-Ti-O fleion vibrations.

The optical and structural properties of nanoparticles are often investigated by UV-Vis adsorption spectrophotometer. The UV diffused absorption edge i.e., the optical absorption property of the material and migration of the light induced electrons and holes are considered as the key factor controlling the photocatalytic

properties of the nanoparticles. Of course, these migrations are relevant to the change in the electronic structure and characteristic of the material. The UV-Vis spectra (figure 4) indicates a strong light absorption in the UV region, but marked peaks around 430nm (absorption in the visible region) were observed for doped TiO_2 nanoparticles which are ascribed to the charge transfer from the valence band (2p orbital of TiO_2) to the conduction band (3d orbital of the Ti^{4+}) for both doped and un-doped nanoparticles. Thus decrease in the band gap was possible by doping with Pd, Pt and Pd/Pt ions which were substituted into TiO_2 lattice of nanoparticles which was confirmed from XRD studies.

The XRD patterns of undoped TiO_2 from (figure 5a) was consistent with the standard crystal structure of TiO_2, (figure 5b-d) shows no diffraction peaks associated with any of the doped ions which is due to the doping of low amount of dopants that being below the detection limit and also it indicates that specific dopant can be considered as fully incorporation into TiO_2 lattice. There are no Pd metal or PdO and Pt metal or PtO or PtO_2 diffraction lines in the XRD profile confirming Pd, Pt and Pd/Pt ion substitution in TiO_2 nanoparticles. This indicates that no significant change has occurred when the Ti^{+4} ions were replaced by Pt^{+4}, may be due to the similarity of their ionic radii which is equal to(0.605Å) for Ti^{+4} and (0.80 Å) for Pt^{+2} and (0.625 Å) for Pt^{+4} in octahedral coordination with oxygen [40,41]. So the Pt^{+4} ions are most likely to be substituted directly in Ti^{+4} sites and it can bond with the surrounding oxygen atoms without distortion. In case of Pd doped TiO_2, there is very little change in the lattice parameters compared to pure anatase TiO_2 as ionic radius of Pd^{+2} ion in square planar coordination is (0.64 Å) [41] which is close to Ti^{+4} ion in octahedral coordination. The XRD patterns of undoped TiO_2 and M/ TiO_2 (M=Pd, Pt, Pt/Pd) doped sample, indicate that the doping of metals had no deleterious effect on the crystal phase of TiO_2 which was further studied by DLS and Zeta potential of the nanoparticles.

Dynamic light scattering (DLS) provides insight into the dynamic properties of soft materials by measuring single scattering events, meaning that each detected photon has been scattered by the sample exactly once. In particular, DLS measurements were performed on TiO_2 and M/ TiO_2 (M=Pd, Pt, Pt/Pd) doped colloidal dispersion solution, after filtering the solutions through a 0.45μm filter (Merck Millipore), in order to estimate size at 25°C. Samples were prepared by centrifugation, in order to remove dust and artifacts from the solution. Following ultrasonication, characterization of nanoparticles like particle size and Zeta potential was performed to explore properties of the materials, which confirmed that all the undoped and doped nanoparticles had similar range of size and small varied potential.

Generally, the bactericidal and fungicidal effect of TiO_2 and M/ TiO_2 (M=Pd, Pt, Pt/Pd) nanoparticles has been attributed to the decomposition of bacterial outer membranes by reactive oxygen species (ROS), primarily hydroxyl radicals (OH^-), which leads to phospholipids peroxidation and ultimately cell death [43] which made the synthesized nanoparticles as good antibacterial and antifungal agents.

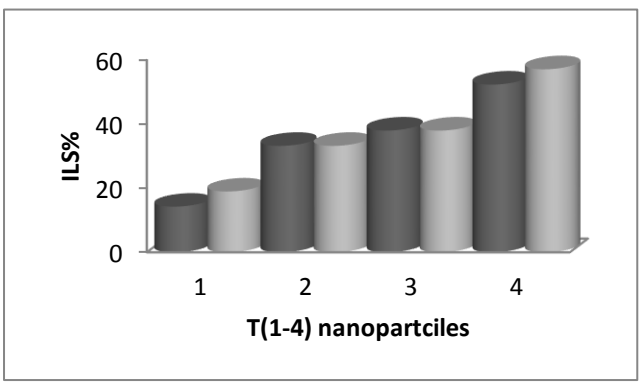

Figure 8: Plot of TiO_2 and M/ TiO_2 (M=Pd, Pt, Pt/Pd) doped nanoparticles showing increase in ILS%.

Apoptosis is known as a distinct mode of programmed cell death that involves the elimination of genetically damaged cells. Apoptotic cell death occurs as a defense mechanism when cellular DNA is damaged beyond the repair [44]. Thus the in-vivo acute toxicology test showed that, upon acute exposure, TiO_2 nanoparticles pass through both the follicle-associated epithelium and the regular intestinal epithelium and get localized in the tissues below these epithelial layers. This can be considered as the first stage of translocation. TiO_2 nanoparticles exposure results in an increase of paracellular permeability, certainly via the disruption of cell junctions. Potential of TiO_2 NPs to be applied for different types of cancers, such as leukemia, cervical, liver and lung cancers have been already reported [45,46]. However it is reported that if experiments were processed in the dark, ROS accumulation decreased, suggesting that TiO_2 nanoparticles generated ROS in cells via photo catalysis [47]. Thus the results from the table 4 and (figure 8), suggest that nanoparticles interact with molecules of the cell replication cycle [48].M/ TiO_2 (M=Pd, Pt, Pt/Pd) doped nanoparticles exhibit DNA damage properties thus causing apoptosis in cancer cells.

The available evidences indicate that M/ TiO_2 (M=Pd, Pt, Pt/Pd) doped nanoparticles induce genotoxicity mainly via generating oxidative stress in cancer cells under visible radiations. The ROS generation is dependent

on the size, structure, and aggregation of the M/ TiO_2 (M=Pd, Pt, Pt/Pd) nanoparticles. The oxidative stress produced by the nanoparticles could affect DNA repair, cell cycle progression, cell proliferation, and apoptosis by affecting protein structure. These nanoparticles at small concentration penetrate into cells, they cross the plasma membrane to areas of low concentration of chloride ions intercellular and extracellular. Thus when penetrated they undergo hydrolysis with water or hydroxyl molecules replacing one or more chloride ions. Subsequently tp-DNA intra and inter bonds mainly involving Guanine N(7) to Guanine N(5) are formed and are also arrested at various stages of the cell cycle including G-I stage or G-II stages. Hence TiO_2 undoped and M/ TiO_2 (M=Pd, Pt, Pt/Pd) doped nanoparticles proved that they posses antiproliferation activity without exposure to UV-light as doping reduces the band gap of the TiO_2 nano-particles.

V. Conclusion

Nowadays, there is a great competition in the drug industry for application of novel technologies. Thus, TiO_2 and M/ TiO_2 (M=Pd, Pt, Pt/Pd) doped nanoparticles were successfully synthesized by solution combustion synthesis. Doping of TiO_2 with metal like (M=Pd, Pt, Pt/Pd) has no significant effect on the particle sizes and did not result in the formation of new crystalline phases. On comparing the TiO_2 undoped and M/ TiO_2 (M=Pd, Pt, Pt/Pd) doped nanoparticles photocatalyst as photosensitizers, doped nanoparticles have found to be the most appropriate materials as antibacterial, antifungal and anticancer agents due to their cost effectiveness, biological, chemical inertness, long term stability against corrosion and strong oxidizing power. Doping which shifts the onset wavelength of TiO_2 matrix to higher values (red shift). Thus, our research reports that TiO_2 and M/ TiO_2 (M=Pd, Pt, Pt/Pd) doped nanoparticles posses antibacterial, antifungal and antiproliferation property under visible radiations. Nevertheless, as a suggested future study, it could be of high value to perform similar study in the frame of target drug delivery studies, especially on various cancer cells.

Acknowledgment

The authors would like to thank to Dr.M.S. Hegde, Talent development center, IISC, Kudhapur, Chitra Durga for providing the lab facilities for completion of the synthesis work. Dr. Sharan goudaHiregoudar, UAS, Raichur for providing the lab facilities. Dr. Sridhar Pai, MCOPS Manipal for providing EAC- induced tumor and RGUHS.

Conflict of interest

The authors declare no conflict of interests.

References

[1]. Torre LA, Bray F, Siegel RL, et al. Global cancer statistics, 2012. CA Cancer J Clin. 2015; 65: 87-108.
[2]. G. Zhao and B. L. Rodriguez, "Molecular targeting of liposomal nanoparticles to tumor microenvironment," International Journal of Nanomedicine **8**, 61 (2013).
[3]. Y. Wang, F. Yang, H. X. Zhang, X. Y. Zi, X. H. Pan, F. Chen, W. D. Luo, J. X. Li, H. Y. Zhu, and Y. P. Hu, "Cuprous oxide nanoparticles inhibit the growth and metastasis of melanoma by targeting mitochondria," Cell Death & Disease**4**(8), e783 (2013).
[4]. Lanthanides: Applications in Cancer Diagnosis and TherapyRuijie D. Teo†, John Termini*,‡, and Harry B. Gray*,†
[5]. S. Ganta , H. Devalapally , A. Shahiwala , M. Amiji , J. Control. Release **2008** ,126 , 187 .
[6]. S. Mura , J. Nicolas , P. Couvreur , Nat. Mater. **2013** ,12 , 991 .
[7]. T. M. Allen , P. R. Cullis , Science **2004** , 303 , 1818 .
[8]. S. Sortino ,J. Mater. Chem. **2012** ,22 , 301 .
[9]. Y. Min , J. Li , F. Liu , E. K. L. Yeow , B. Xing , Angew. Chem., Int. Ed. **2014** ,53 , 1012 .
[10]. L. Cheng , K. Yang , Y. Li , J. Chen , C. Wang , M. Shao , S. T. Lee , Z. Liu , Angew. Chem., Int. Ed. **2011** ,50 , 7385 .
[11]. K. Szaciłowski , W. Macyk , A. Drzewiecka-Matuszek , M. Brindell , G. Stochel , Chem. Rev. **2005** , 105 , 2647 .
[12]. Y. Yang , Q. Shao , R. Deng , C. Wang , X. Teng , K. Cheng , Z. Cheng , L. Huang , Z. Liu , X. Liu , B. Xing , Angew. Chem., Int. Ed. 2012 ,51 ,3125 .
[13]. Shi, H., Magaye, R., Castranova, V. & Zhao, J. Titanium dioxide nanoparticles: a review of current toxicological data. Part. FibreToxicol. **10**, 15 (2013).
[14]. Wu, K. C. et al. Biocompatible, surface functionalized mesoporous titania nanoparticles for intracellular imaging and anticancer drug delivery. Chem Commun (Camb) **47**, 5232–5234 (2011).
[15]. Xie, Q. et al. Nanosheet-based titania microspheres with hollow core-shell structure encapsulating horseradish peroxidase for a mediator-free biosensor. Biomaterials **32**, 6588–6594 (2011).
[16]. Paunesku, T. et al. Biology of TiO2-oligonucleotide nanocomposites. Nat. Mater. **2**, 343–346 (2003).
[17]. Trouiller, B., Reliene, R., Westbrook, A., Solaimani, P. &Schiestl, R. H. Titanium dioxide nanoparticles induce DNA damage and genetic instability in vivo in mice. Cancer Res. **69**, 8784–8789 (2009).
[18]. Wu, J. et al. Toxicity and penetration of TiO_2 nanoparticles in hairless mice and porcine skin after sub chronic dermal exposure. Toxicol. Lett. **191**, 1–8 (2009).
[19]. Ghosh, M., Bandyopadhyay, M. & Mukherjee, A. Genotoxicity of titanium dioxide (TiO_2) nanoparticles at two trophic levels: Plant and human lymphocytes. Chemosphere **81**, 1253–1262 (2010).

[20]. Bhattacharya, K. et al. Titanium dioxide nanoparticles induce oxidative stress and DNA-adduct formation but not DNA-breakage in human lung cells. Part. FibreToxicol. **6**, 17 (2009).
[21]. Kocbek, P., Teskac, K., Kreft, M. E. &Kristl, J. Toxicological aspects of long-term treatment of keratinocytes with ZnO and TiO_2 nanoparticles. Small **6**, 1908–1917 (2010).
[22]. Hackenberg, S. et al. Functional responses of human adipose tissue-derived mesenchymal stem cells to metal oxide nanoparticles in vitro. J. Biomed. Nanotechnol. **9**, 86–95 (2013).
[23]. Iavicoli, I., Leso, V., Fontana, L. & Bergamaschi, A. Toxicological effects of titanium dioxide nanoparticles: a review of in vitro mammalian studies. Eur. Rev. Med. Pharmacol. Sci. **15**, 481–508 (2011).
[24]. Lang, X. J., Chen, X. D. & Zhao, J. C. Heterogeneous visible light photocatalysis for selective organic transformations. Chem. Soc. Rev.**43**, 473–486 (2016).
[25]. Xuming, Z., Yu, C., Ru-Shi, L. & Ping, T. Plasmonic photocatalysis. Rep. Prog. Phys. **76**, 046401 (2013).
[26]. Zhang, S., Yang, D., Jing, D., Liu, H., Liu, L., Jia, Y., ... &Huo, Z. (2014). Enhanced photodynamic therapy of mixed phase TiO_2 (B)/anatase nanofibers for killing of HeLa cells.
[27]. Nano Research, 7(11), 1659-1669.
[28]. Jang, H., Choi, M. H., Yim, Y., Kim, Y. K., & Min, D. H. (2015). Cancer Treatment: Dual- Wavelength Irradiation and Dox Delivery for Cancer Cell Ablation with Photocatalytic Pr Doped TiO_2/NGO Hybrid Nanocomposite (Adv. Healthcare Mater. 12/2015). Advanced healthcare materials, 4(12), 1736-1736.
[29]. Feng, N. et al. Understanding the High Photocatalytic Activity of (B, Ag)-Codoped TiO_2 under Solar-Light Irradiation with XPS, Solid-State NMR, and DFT Calculations. J. Am. Chem. Soc. **135**, 1607–1616 (2013).
[30]. Jiang, Z. F. et al. Silver-loaded nitrogen-doped yolk–shell mesoporous TiO_2 hollow microspheres with enhanced visible light photocatalytic activity. Nanoscale **7**, 784–797 (2015).
[31]. Boxi, S. S., Mukherjee, K. &Paria, S. Ag-doped hollow TiO_2 nanoparticles as an effective green fungicide against Fusarium solani and Venturia inaequalis phytopathogens. Nanotechnology **28**, 085103 (2016).
[32]. Paul, K. K., Ghosh, R. &Giri, P. K. Mechanism of strong visible light photocatalysis by Ag2O-nanoparticle-decorated monoclinic TiO_2(B) porous nanorods. Nanotechnology **27**, 315703 (2016).
[33]. Lin, Y. et al. Synthesis of Ag/TiO_2 core/shell nanoparticles with antibacterial properties. Bull. Korean Chem. Soc. **32**, 2607–2610 (2011).
[34]. Dalai, S., Pakrashi, S., Kumar, R. S., Chandrasekaran, N. & Mukherjee, A. A comparative cytotoxicity study of TiO_2 nanoparticles under light and dark conditions at low exposure concentrations. Toxicol. Res. **1**, 116–130 (2012).
[35]. CLSI. Methods for Antimicrobial Susceptibility Testing for Human Mycoplasmas: Approved Guideline. CLSI document M43-A. Wayne, PA: Clinical and Laboratory Standards Institute; 2011.
[36]. Berne BJ, Pecora R. Dynamic Light Scattering. Mineola (NY): Courier Dover; 2000.
[37]. Shannon RD. Revised effective ionic radii and systematic studies of interatomic distances in halides and chalcogenides. Acta Cryst. A. 1976;32:751-767.
[38]. D'Souza, L.P., Shree, S. and Balakrishna, G.R. (2013) Bifunctional Titania Float for Metal Ion Reduction and Organics Degradation, via Sunlight. Industrial & Engineering Chemistry Research, **52**, 16162-16168. http://dx.doi.org/10.1021/ie402592k
[39]. Buha J. Solar absorption and microstructure of C-doped and H co-doped TiO2 thin films. J. Phys. D, Appl. Phys. 2012;45:385305.
[40]. Thompson T L, Yates Jr J T. Surface science studies of the photoactivation of TiO2-New photochemical processes. Chem Rev, 2006, 106: 4428–4453
[41]. Roy,M.S.Hegde, N.Raishankar,G.Madras,J.Phy.Chem C111.8153(2007).
[42]. J.E.Huheey,InorganicChemistry,Principles of Structure and Reactivity, 3rd edition, Harper and Row, New York,pp129(1983).
[43]. B. D. Cullity, 1978 Elements of X-Ray Diffraction, Adison-Wesley.
[44]. C.Jayaseelan, A.A. Rahuman, S.M. Roopan, A.V. Kirthi, J. Venkatesan, S.Kim, M. Iyappan, C. Siva. "Biological approach to synthesize TiO2 nanoparticles using Aeromonas hydrophila and its antibacterial activity." Spectrochimica Acta Part A: Molecular and Biomolecular Spectroscopy, vol. 107, pp. 82–89, Apr. 2013.
[45]. Xue, Y. et al. Cytotoxicity and apoptosis induced by silver nanoparticles in human liver HepG2 cells in different dispersion media. J. Appl. Toxicol. **36**, 352–360 (2016).
[46]. Lagopati, N. et al. Effect of nanostructured TiO(2) crystal phase on photoinduced apoptosis of breast cancer epithelial cells. Int. J. Nanomedicine **9**, 3219–3230 (2014).
[47]. Wang, Y. et al. Cytotoxicity, DNA damage, and apoptosis induced by titanium dioxide nanoparticles in human non-small cell lung
[48]. cancer A549 cells. Environ. Sci. Pollut. Res. Int. **22**, 5519–5530 (2015).
[49]. Hoshino A, Fujioka K, Oku T, et al. Physicochemical properties and cellular toxicity of nanocrystal quantum dots depend on their surface modification. Nano Lett. 2004;4:2163–2169.
[50]. Magdolenova Z, Bilani_cova´ D, Pojana G, et al. Impact of agglomeration and different dispersions of titanium dioxide

* Veena.V TiO_2 And Pt/Pd Doped TiO_2 Upconversion Nanoparticles For Photodynamic Biomedical Applications." IOSR Journal of Pharmacy and Biological Sciences (IOSR-JPBS) 13.5 (2018): 01-10.